



Multi-diffractive grating for surface plasmon biosensors with direct back-side excitation

SIMONE HAGENEDER,¹ STEFAN FOSSATI,¹ NICOLAS-GUILLERMO FERRER,^{1,2} BATUHAN GÜNGÖRMEZ,^{1,3} SIMONE K. AUER,^{1,4} AND JAKUB DOSTALEK^{1,5,*} 

¹AIT-Austrian Institute of Technology GmbH, Konrad-Lorenz-Strasse 24, Tulln 3430, Austria

²University of Tokyo, Department of Advanced Materials Science, Kashiwanoha 5-1-5, Kashiwa, Chiba 277-8561, Japan

³Department of Materials Science and Engineering, Gebze Technical University, Gebze, Kocaeli, Turkey

⁴CEST Kompetenzzentrum für elektrochemische Oberflächentechnologie GmbH, TFZ, Wiener Neustadt 2700, Austria

⁵FZU-Institute of Physics, Czech Academy of Sciences, Na Slovance 2, Prague 182 21, Czech Republic

*jakub.dostalek@ait.ac.at

Abstract: A multi-diffractive nanostructure is reported for the resonant excitation of surface plasmons that are cross-coupled through a thin metallic film. It consists of two superimposed periodic corrugations that allow diffraction excitation of surface plasmons on the inner side of a thin metal film and their subsequent phase matching with counterpropagating surface plasmons travelling to the opposite direction on its other side. This interaction leads to establishing of a set of cross-coupled Bragg-scattered surface plasmon modes that exhibit an electromagnetic field localized on both metal film interfaces. The reported structure is attractive for surface plasmon resonance biosensor applications, where direct optical probing can be done through the substrate without the need of optical matching to a high refractive index prism. In addition, it can be prepared by mass production – compatible means with UV-nanoimprint lithography and its biosensing performance characteristics are demonstrated by refractometric and biomolecular affinity binding studies.

© 2020 Optical Society of America under the terms of the [OSA Open Access Publishing Agreement](#)

1. Introduction

Metallic nanostructures increasingly serve for optical probing of biomolecules and their interactions in important fields of analytical technologies and life science research. They allow for the resonant coupling of light to surface plasmon modes originating from collective oscillations of electron density and associated electromagnetic field that is tightly confined on the metallic surface. Such confinement of electromagnetic field leads to the enhancement of its intensity and local density of optical states, and it has been exploited in surface plasmon resonance (SPR) biosensors [1] as well as for the amplification of weak optical spectroscopy signal including Raman scattering [2], fluorescence [3] and near-infrared absorption [4].

The majority of SPR biosensors utilize sensor chips with a thin metallic film supporting propagating surface plasmons (PSPs). In Kretschmann configuration of attenuated total internal reflection (ATR) method, these sensor chips are optically matched to an optical prism for the coupling of PSPs at the outer side of the metallic film with an optical beam travelling through the sensor chip substrate [5]. The outer sensor surface is brought in contact with an analyzed liquid sample, and the molecular binding events are observed by interrogating resonant excitation of PSPs in the wavelength [6] or angular [5] reflectivity spectrum. Alternative approaches based on diffraction grating-based excitation of PSPs [7] were pursued, and also metallic nanostructures supporting localized surface plasmons (LSPs) [8] were used to avoid the optical matching of sensor chips to bulky ATR prism. The wavelength interrogation of LSPs can be utilized from both

sample and sensor chip sides in transmission [9] or reflection mode [10]. This measurement can be performed by dedicated instruments [11] and also by using already established optical readers deployed in standard molecular biology laboratories. These particularly include microtiter plates where the bottom wells carry adsorbed gold nanoparticles prepared by chemical synthesis [12] and thin metallic films perforated with arrays of nanoholes by lithography [13,14].

In general, the measurement in reflection mode from the substrate side of a sensor chip carrying plasmonic nanostructures offers the advantage of avoiding passing the probing optical beam through the analyzed liquid sample. This back-side coupling allows for rapid direct analysis of complex matrices (such as minimally processed blood) that absorb or scatter light. Also, it offers improved stability for the *in situ* SPR measurements, which otherwise require using of transparent flow-cells and make the measurements prone to respond to the sample flow fluctuations. The separation of the fluidic and the optical parts of the plasmonic sensor chip was reported by cross-coupled PSP modes on thin gold films that are perforated with arrays of nanoholes and attached to a low refractive index dielectric film [15]. This configuration takes advantage of refractive index symmetrical geometry that enables cross-coupling of PSP at opposite interfaces leading to the establishment of long-range surface plasmon modes [16]. Another possible approach to diffraction-based excitation of PSPs on non-conformal diffraction gratings was demonstrated on metallic films that were corrugated only on inner side [17]. However, the preparation of such nanostructures for back-side excitation of coupled PSPs or LSPs can be only prepared by using methods involving multiple lithography steps. Typically, periodic arrays of plasmonic nanoholes and discs are prepared by electron beam lithography, which offers precise control of the nanostructure geometry. However, it represents an approach relying on complex infrastructure that is suitable only for research as the fabrication over larger areas $> 100 \mu\text{m}$ is slow. Among others, UV-laser interference lithography [18] and UV-nanoimprint lithography combined with lift-off [19], dry etching steps [20], or template stripping [21,22] have been proposed, but they elevate this limitation only partially.

In this paper, we report on a new approach for back-side excitation of PSPs based on multi-periodic gratings (MPG) coated with a thin metallic film. The structure is based on a corrugation profile with multiple superimposed relief periodic modulations that have been explored before for the broadband plasmonic absorbers [23], multi-resonant plasmonic nanostructures for the amplification of weak fluorescence signal [24], and SPR biosensors with Bragg-scattered surface plasmons [25]. We report for the first time on tailoring this geometry for the cross-coupling of PSPs across a thin metallic film and implement it for real-time *in situ* observation of molecular binding-induced refractive index changes based on detuning of the tailored plasmonic resonance that is measured with the back-side excitation geometry.

2. Materials and methods

2.1. Preparation of multi-diffractive grating structures

The MPG structure was recorded by UV laser interference lithography (UV-LIL) with Lloyd's mirror configuration. Positive photoresist Microposit S1805 from Microchem (USA) was spun on a BK7 glass substrate at 4500 rpm for 45 seconds (yielding a thickness of 500 nm) and dried on a hot plate at 98 °C for 120 sec. Afterwards, the substrate was mounted to the UV-LIL setup and exposed to the field of two interfering collimated beams (with an intensity of $32 \mu\text{W cm}^{-2}$) emitted from a HeCd laser IK 3031 R-C from Kimmon (Japan) at wavelength $\lambda=325 \text{ nm}$. The angle of the interfering beams was set to $69^{\circ}05'$ and $47^{\circ}10'$ deg, which corresponds to periods of $\Lambda_1=455$ and $\Lambda_2=239 \text{ nm}$, respectively. To record the MPG structure, the photoresist layer was sequentially exposed to the interference field at each respective angle. For the preparation of crossed gratings, the sequential exposure to interference field was carried out twice for two orientations of the sample rotated by 90 degrees. The relief corrugation was etched into the photoresist by a developer AZ 303 from MicroChemicals (Germany) diluted by distilled water at

a ratio of 1:15. For the measurements discussed below, we used a grating C2.2.ABPO with a recording time of the period Λ_1 of 10 min, recording time of the period Λ_2 of 25 min, and the development time 90 s.

Prepared photoresist grating was cast to polydimethylsiloxane (PDMS) Sylgard 184 from Dow Corning (USA). Multiple generation copies were prepared, and PDMS was cured at elevated temperature to fine-tune the periods and the modulation depth of the recorded structure and to serve as a working stamp after the detachment of the cured polymer. Cleaned BK7 glass substrates were coated with the UV-curable polymer Amonil MMS 10 from AMO GmbH (Germany) by spin-coating at 3000 rpm for 120 s. Then, the PDMS working stamp was placed on the top of the fluid Amonil layer and, after 5 min rest time, irradiated by UV light with a dose of 2 J cm^{-2} (UV lamp Bio-Link 365, Vilber Lourmat). Finally, the PDMS working stamp was detached from the UV-cured Amonil MMS 10, leaving a copy of the master structure on the glass substrate. The copied MPG structure was placed on a hot plate at $120 \text{ }^\circ\text{C}$ for 4 min, then coated with 50 nm of gold by vacuum thermal evaporation by using an instrument HHV AUTO 306 from HHV Ltd (UK) in vacuum better than 10^{-6} mBar.

2.2. Optical setup

A polychromatic light beam emitted from a halogen light source LSH102 from LOT-Oriel (Germany) was coupled to a multimode optical fiber M25L02 from Thorlabs (UK). The beam emitted from the optical fiber end was collimated by using a lens with $f=30$ mm and made normally incident at the gold MPG surface through the glass substrate. The reflected beam was collected from a multimode optical fiber M26L02 from Thorlabs (UK) by using a collimator F810SMA-635 from Thorlabs (UK) and delivered to a spectrometer HR4000 from Ocean Optics (USA) or Shamrock 303i from Andor (USA). Raw wavelength spectra of the light beam reflected from the MPG surface were normalized with a spectrum acquired for a reference flat gold surface. A flow-cell was clamped against the grating sensor chip, and it consisted of a polished plastic substrate with drilled input and output ports and a thin PDMS gasket. The volume of the flow-cell was $10 \text{ }\mu\text{L}$, and analyzed liquid samples were flowed through by using the peristaltic pump REGLO Digital MS-4/8 from Ismatec (Switzerland) and tubing with a 0.64 mm inner diameter from Ismatec Wertheim (Germany) at a flow rate of $80 \text{ }\mu\text{L}/\text{min}$. The sensing spot in the flow-cell was illuminated by a polychromatic beam with a diameter of about 5 mm. The normalized reflectivity spectra were evaluated by a dedicated software developed in-house by using LabView from National Instruments (USA). The sequentially acquired specular reflectivity spectra $R_0(\lambda)$ were processed by a routine centroid [26] in the selected wavelength range $\lambda_{n1} - \lambda_{n2}$ in order to track the refractive index changes in realtime. The reflectivity spectra $R_0(\lambda)$ were acquired with an integration time of 5 ms and the accumulation of 300 was used to reduce noise. The centroid wavelength was determined from discrete reflectivity values $R_0(\lambda_i)$ as:

$$\lambda_{\text{cen}} = \frac{\sum_{i=N_1}^{N_2} \lambda_i [R_t - R_0(\lambda_i)]}{\sum_{i=N_1}^{N_2} [R_t - R_0(\lambda_i)]}, \quad (1)$$

where N_1 and N_2 are indexes that define pixels over which the centroid routine was applied, λ_i is the wavelength corresponding to the i^{th} detector pixel, and R_t is a threshold.

2.3. Optical simulations

Finite element method was employed as implemented in a diffraction grating solver DiPoG (Weierstrass Institute, Germany). A grating in a computation cell with a length of up to $\Lambda=4.6 \text{ }\mu\text{m}$ and height $1 \text{ }\mu\text{m}$ was approximated by a mesh of triangles (convergence check was performed by increasing the number of triangles). Cartesian coordinates with the x and z axes in the plane of the MPG structure and y -axis perpendicular to the MPG structure were used as seen in Fig. 1(a).

The corrugation profile with two superimposed relief gratings (period $\Lambda_1=0.46\ \mu\text{m}$ and $\Lambda_2=0.242\ \mu\text{m}$) and were defined as higher harmonics: $y = a_1 \sin(2\pi/\Lambda_1 \cdot n_1 \cdot x) + a_2 \sin(2\pi/\Lambda_2 \cdot n_2 \cdot x)$, where a_1 and a_2 states for amplitudes and $n_1=10$ and $n_2=19$. In the used numerical model, the set of Maxwell equations was solved by using the PARDISO solver of sparse linear systems developed at University of Basel (Switzerland).

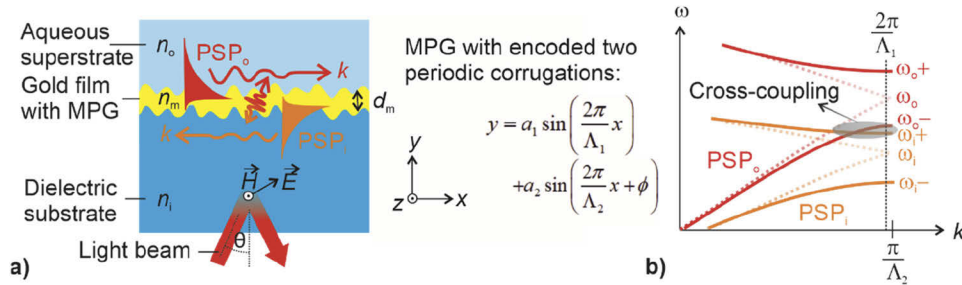


Fig. 1. Schematics of a) the cross-coupling of PSPs across a thin metallic film on an MPG with encoded longer period Λ_1 and shorter period Λ_2 . b) Schematics of the dispersion relation of PSPs at the outer and inner interfaces that is folded into first Brillouin zone.

2.4. Biomolecular binding study

After the deposition of 50 nm thick gold layer to the MPG surface, its surface was modified with a self-assembled thiol monolayer (SAM) by immersion in ethanolic solution with dissolved thiols carrying functional biotin (0.2 mM HS-C11-EG6-Biotin) and passivating oligoethylene glycol groups (0.8 mM HS-C11-EG6-OH) from Prochimia Surfaces in Gdynia (Poland). After overnight incubation, the substrates with MPG were rinsed with ethanol, dried in a stream of nitrogen and stored in argon atmosphere until further use. For the affinity binding measurements, a flow cell was clamped onto the surface of the MPG, and phosphate-buffered saline (137 mM NaCl, 2.7 mM KCl, 12 mM phosphate buffer, pH 7.4, no. E504) from VWR (USA) spiked with 0.05% Tween 20 BioXtra, from SigmaAldrich, (USA) (PBST) was flowed until a stable baseline of the sensor response λ_{cen} is reached. Then, the calibration was done using PBST spiked with sucrose at concentrations of 1, 2 and 4%. Afterwards, the surface was reacted with neutravidin (NA) from Thermo Scientific (Austria) and biotinylated monoclonal capture antibody cAB #13-7349-81 from eBioscience (Austria). This antibody is specific to human tumor necrosis alpha (TNF- α) BMS301 from eBioscience (Austria), and a sandwich immunoassay format was implemented by using a secondary monoclonal antibody sAB against another part of TNF- α #14-7348-81 from eBioscience (Austria).

3. Results and discussion

In order to resonantly excite PSP modes that are cross-coupled through a thin gold film, a relief profile of MPG with two superimposed periodic corrugations is investigated. As illustrated in Fig. 1(a), there is assumed the geometry where a collimated optical beam is travelling through a dielectric substrate (refractive index of glass n_i) and impinges on a corrugated thin gold film (refractive index n_m , thickness of d_m). A normally incident beam ($\theta=0$) is coupled to the PSPs at the inner interface between the substrate n_i and gold n_m by the first-order diffraction on grating corrugation component with a period Λ_1 . In general, this corrugation component also allows to couple the incident beam to PSP modes travelling along the outer interface between the gold film n_m and a lower refractive index dielectric (water with refractive index n_o). However, the coupling efficiency is negligible as the majority of the incident beam intensity is reflected at an

inner interface with the substrate n_i and does not reach the opposite interface in contact with the superstrate n_o .

To solve this problem, additional corrugation component with a shorter period Λ_2 was superimposed over the corrugation with the period Λ_1 . As schematically indicated in the PSP dispersion relation folded to the first Brillouin zone in Fig. 1(b), the introduction of shorter Λ_2 can be utilized for its splitting at the outer and inner interfaces so new Bragg-scattered PSPs occur at distinct wavelengths (represented by frequencies ω_i and ω_o) with an optical bandgap in between. These Bragg-scattered modes are further noted as ω_+ and ω_- and they are associated with diffraction coupling of counter-propagating PSP modes on the corrugation component Λ_2 at individual interfaces generating standing wave-like modes [27]. In general, the spectral width of the optical bandgap in the dispersion relation of PSP modes at ω_i and ω_o can be tuned, so the short-wavelength Bragg-scattered PSP on the inner interface ω_i^+ overlaps with the long-wavelength Bragg-scattered PSP on the outer interface ω_o^- . Then, these modes become phase-matched along the surface and allow to transfer the electromagnetic field intensity through the metallic film via their penetrating evanescent field tails.

This concept was firstly analyzed by using numerical simulations. In this study, a thickness of the gold film of $d_m=50$ nm was assumed with conformally corrugated interfaces between the substrate with refractive index $n_i=1.5$ (BK7 glass) and superstrate with lower refractive index $n_o=1$ (air) and $n_o\sim 1.33$ (water). There was used relief profile composed of sinusoidal corrugation with a longer period $\Lambda_1=460$ nm superimposed over additional sinusoidal corrugation exhibiting a shorter period $\Lambda_2=242$ nm. Firstly, we simulated zero-order reflectivity spectrum R_0 for the corrugation profile, in which the amplitude for the long period Λ_1 component was set to $a_1=10$ nm and the shorter period component Λ_2 was not present by assuming $a_2=0$ nm. Then, the first order excitation of the PSP mode at the inner interface occurs and manifests itself as a dip in the wavelength spectrum of R_0 centered at a wavelength $\lambda_i=745$ nm, Fig. 2(a). When increasing the refractive index of the dielectric at the outer interface from $n_o=1.33$ to 1.35, a negligible shift in the resonance wavelength $\delta\lambda_i=0.7$ nm occurs as the majority of the field intensity associated with this resonance is confined at the opposite inner interface with the glass substrate [see the profile of magnetic field amplitude in Fig. 2(c)].

When introducing the shorter period component Λ_2 forming the complete MPG structure with the amplitudes $a_1=10$ and $a_2=10$ nm, the resonance at λ_i splits and two overlapping dips occur at wavelengths of $\lambda_{i1}=724$ and $\lambda_{i2}=744$ nm. Interestingly, when increasing the refractive index at the outer interface from $n_o=1.33$ to 1.35, both resonances shift by about 6.5 nm and the coupling strength to shorter wavelength resonance λ_{i1} increases while that to λ_{i2} decreases, Fig. 2(b). The reason that the split resonance can be efficiently detuned by the refractive index change at the outer interface n_o is due to the fact that the associated field profile is confined at both interfaces as cross-coupling of PSPs through the metallic film occurs, Fig. 2(c). Notably, the coupling strength to the cross-coupled PSPs is decreased compared to the geometry when PSPs travelling on the individual interface are excited with the selected corrugation amplitude a_1 . The coupling strength can be optimized by tuning this parameter as indicated by the following experimental study.

Experimentally, the MPG structure was prepared by sequential recording of the periodic interference field with periods Λ_1 and Λ_2 into a photoresist layer by using UV-LIL. The corrugation profile was then etched to the layer by a developer, and the tuning of modulation depths a_1 and a_2 was facilitated by controlling the irradiation time of each step and by the adjusting development time. Afterwards, the structure was cast to PDMS in order to serve as a working stamp, and multiple copies were prepared by transferring the corrugation to a UV-curable polymer Amonil followed by the coating with a gold film with a thickness of $d_m=50$ nm. The corrugation profile was observed by atomic force microscopy (AFM), as presented in Fig. 3(a). It shows a crossed structure where the MPG corrugation profile was recorded in both x and z directions and the fast Fourier transform analysis presented in Fig. 3(b) revealed the parameters of $\Lambda_1=462.0$ nm,

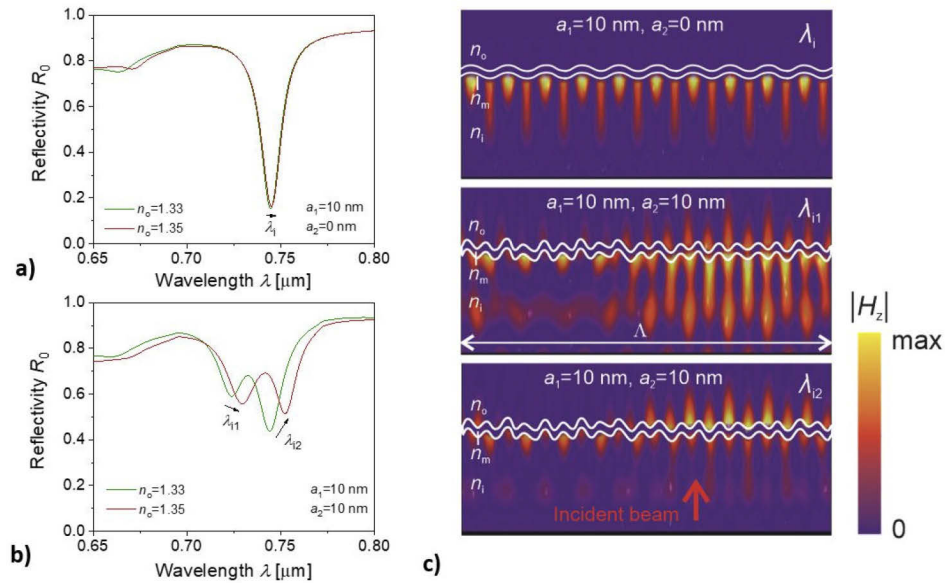


Fig. 2. Simulated reflectivity R_0 for transverse magnetically polarized normally impinging beam from a substrate at the structure with a) encoded single period ($a_1=10$ nm, $a_2=0$ nm) and b) two periods ($a_1=10$ nm, $a_2=10$ nm). c) Near field distribution of magnetic field intensity $|H_z|$ in the xy plane at wavelength λ_i , λ_{i1} and λ_{i2} . The simulations were carried out for a super-period $\Lambda=4.6$ μm , longer period $\Lambda_1=460$ nm, shorter period $\Lambda_2=242$ nm, and $n_0=1.33$.

$\Lambda_2=236.4$ nm, $a_1=13$ nm and $a_2=4$ nm. It is worth of noting that the period Λ_1 was selected to slightly deviate from the $2\Lambda_2$ (as was originally studied on gratings with photonic bandgap [28]) in order to lift out the sensitivity on the mutual phase between these corrugations ϕ . The reason is that the used UV-LIL recording of the MPG structure does not allow for controlling this parameter and by introducing a small offset the phase dependence is averaged when irradiating surface with area at mm^2 scale.

The MPG structure on a glass substrate was used as a sensor chip, and its top outer surface was clamped against a flow-cell, see Fig. 3(c). Then, a polychromatic light beam was made reflected from the inner surface of the gold film on the sensor chip and its spectrum was analyzed by a spectrometer. As described further, there were observed changes in the specular reflectivity spectrum $R_0(\lambda)$ due to the variations of the refractive index of a liquid n_0 flowed through the flow-cell as well as upon refractive index changes induced by molecular binding events. Reflectivity spectra $R_0(\lambda)$ were firstly measured for refractive index $n_0=1$ (air was present in the flow-cell) and $n_0=1.33$ (water was flowed through the flow-cell), Fig. 4(a). In contact with air, reflectivity spectra measured from the inner substrate side (BK7 glass) and the outer superstrate side (flow-cell) show resonances manifested as a dip in $R_0(\lambda)$. For the inner substrate side, the dip is centered at a wavelength close to 720 nm (red curve, ω_{i+}) which is spectrally separated from that observed from the superstrate outer side at 575 nm (blue curve, ω_{o-}). When increasing the outer refractive index to $n_0=1.33$, the reflectivity spectrum $R_0(\lambda)$ measured from the inner superstrate side (green curve) changes and exhibits two spectrally separated dips. These two dips are located at wavelengths of 650 nm (ω_{o+}) and 720 nm (ω_{o-}), and they can be interpreted as first-order diffraction coupling by the corrugation component Λ_1 to PSP modes that are Bragg-scattered on the outer interface by the corrugation component Λ_2 . Importantly, the spectral position of the resonance ω_{o-} is coincident with ω_{i+} that is observed when probing from the inner substrate

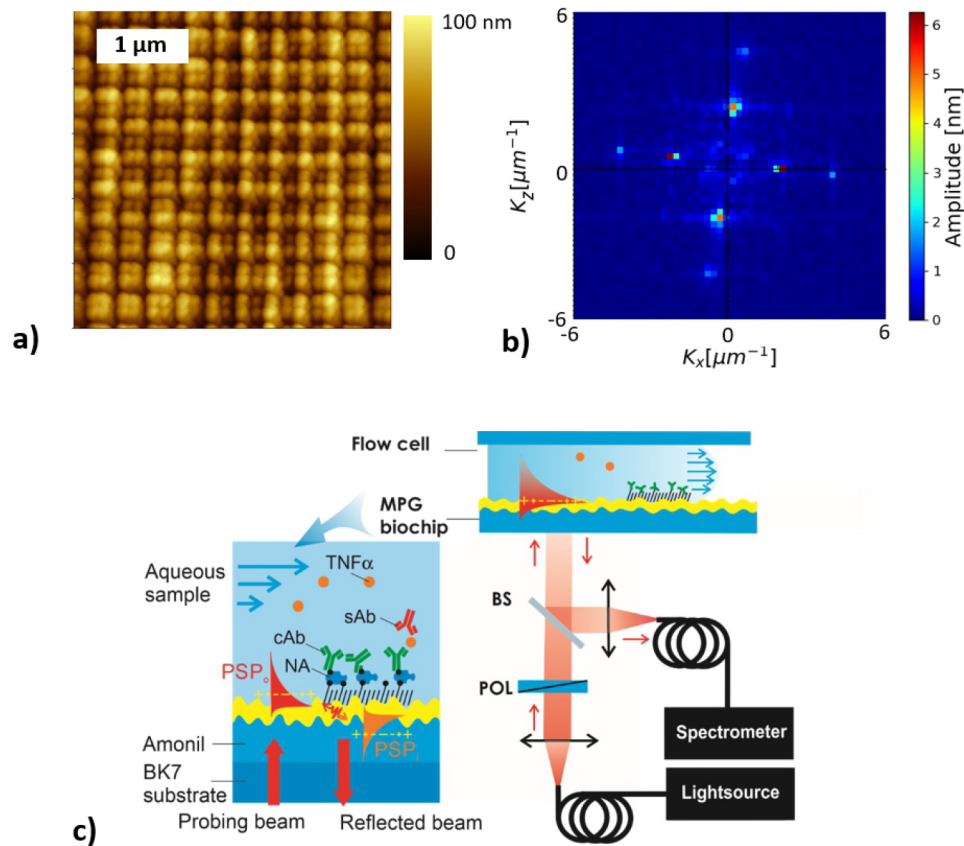


Fig. 3. a) AFM observation of the topography of the prepared MPG corrugation carrying the recorded corrugation with longer period $\lambda_1=462$ nm, $a_1=13$ nm and shorter period $\lambda_2=236.4$ nm, $a_2=10.5$ nm as determined by b) Fourier transform analysis. c) Schematics of the sensor chip with the MPG corrugation and the optical setup for the measurement of spectral reflectivity R_0 with beam splitter (BS) and polarizer (POL).

side. Therefore, the overlaid resonance shows a character of two superimposed Lorentzian dips. A similar profile is observed when the reflectivity $R_0(\lambda)$ is measured from the inner substrate side (black curve), which further confirms that a cross-coupling of PSP modes through the metallic film occurs as predicted by the simulations in Fig. 2(b). The small deviations in the measured resonance spectral position and the stronger coupling can be attributed to the effect of roughness of the gold film that was not taken into account in the mode, increased modulation amplitude a_1 , and possible differences in the optical constants of used thin films.

In order to investigate this phenomenon in more detail, the bulk refractive index of the aqueous solution on the outer surface of the sensor chip was changed from $n_0=1.33$ to 1.38, and the reflectivity $R_0(\lambda)$ was measured from the inner substrate side. As Fig. 4(b) shows, the spectral shape of the resonance dip changes and the lower wavelength component (centered at λ_{i1}) red shifts and become more pronounced. The longer wavelength part (centered at λ_{i2}) also red shifts, but its coupling strength decreases when increasing n_0 . This observation is in qualitative agreement with the simulations presented in Fig. 2(b) and confirms that the proposed concept allows for the cross-coupling of PSP modes through the metallic film and to optically monitor changes in the refractive index from the opposite side.

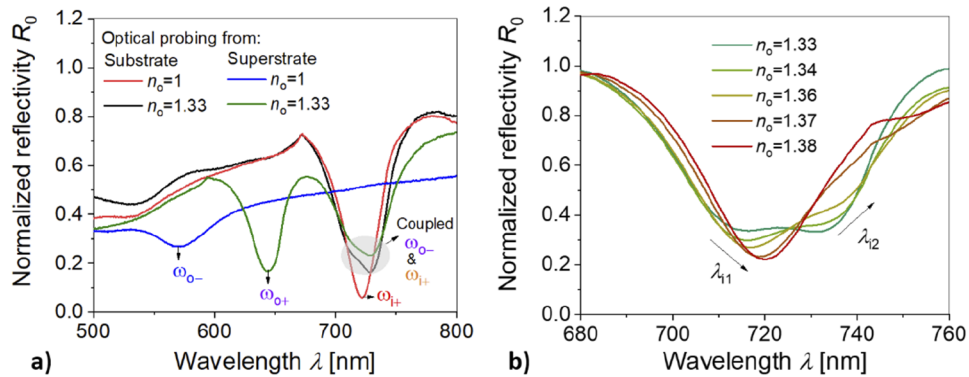


Fig. 4. a) Measured reflectivity R_0 with a beam normally incident at the sensor chip carrying MPG from its substrate (n_i) and superstrate (n_o) sides and air ($n_o=1$) and water ($n_o=1$) on the top. b) A detail of the reflectivity spectrum in the spectral region with cross-coupled surface plasmon resonance and refractive index on the top of the structure varied between $n_o=1.33$ and 1.38.

To implement the developed MPG structure for *in situ* real-time SPR measurements, the reflectivity spectra R_0 were acquired in time, and a centroid method was applied in the spectral region where the cross-coupled SPR dip occurs. This approach was chosen as the variation in the coupling strength to the two overlapped resonances λ_{i1} and λ_{i2} appears to be more pronounced than the spectral shifts $\delta\lambda_{i1}$ and $\delta\lambda_{i2}$. In general, the centroid wavelength λ_{cen} is blue-shifted when increasing the refractive index of the outer dielectric medium n_o , as illustrated in Fig. 5(a). This trend is opposite to classical SPR (where a red shift occurs) due to the observed coupling strength changes of respective dips at λ_{i1} and λ_{i2} . To test the performance of the approach, we tracked the centroid wavelength λ_{cen} in real-time upon changing the bulk refractive index n_o and upon the affinity binding of biomolecules on the gold MPG surface. Before this experiment, the MPG sensor chip was modified by a mixed thiol SAM with biotin head groups. Then the chip was loaded to the optical reader, and a baseline in the sensor signal λ_{cen} was established upon a flow of working buffer PBST, see Fig. 5(b). The centroid threshold parameter was optimized and the best signal-to-noise-ratio was obtained close to $R_t=0.5$, similar to the previous works where a shift in the SPR resonance dip was measured in reflectivity spectra [26]. Afterwards, the PBST solution was spiked with sucrose (1%, 2%, and 4%) and sequentially flowed over the surface to increase the bulk refractive index ($\delta n_o=1.4 \times 10^{-3}$, 2.8×10^{-3} , 5.6×10^{-3} RIU, respectively). As can be seen in Fig. 5(b), the increase in refractive index n_o is accompanied by a stepwise decrease in the sensor signal λ_{cen} , from which a sensitivity of $S_b=\delta\lambda_{cen}/\delta n_o=-252$ nm/RIU was determined. For the baseline noise quantified with a standard deviation of $\sigma(\lambda_{cen})=3.75 \times 10^{-3}$ nm, this sensitivity corresponds to the refractive index resolution of 1.5×10^{-5} . It is worthy of noting that such resolution is comparable to similar sensors with regular grating-coupled SPR (resolution of 6×10^{-6} RIU was reported [29]). The accuracy of the proposed approach is apparently hampered by the fact that the cross-coupled PSP modes travel on both interfaces, while the regular grating-coupled SPR allows for better field confinement by the excitation of PSPs only at individual (active) surface. This can be estimated to reduce the sensitivity (and respectively the refractive index resolution) by a factor of two. Additional parameter that can be used to further optimize the performance of the proposed concept is the thickness of the metal film d_m . In general, decreasing this parameter leads to increasing the coupling strength between the surface plasmon modes travelling along the outer (PSP_o) and inner (PSP_i) by stronger overlapping their field profiles. However, there will also occur an increase in radiative damping of PSP_o that is in general leaky mode into the substrate with higher index of refraction n_i . We assume that then the

spectral width of the coupled resonance will be broadened and the performance characteristics impeded. The chosen thickness of $d_m=50$ nm was selected as the radiative damping is still weak and it already allows to achieve the cross-coupling with the prepared MPG topography.

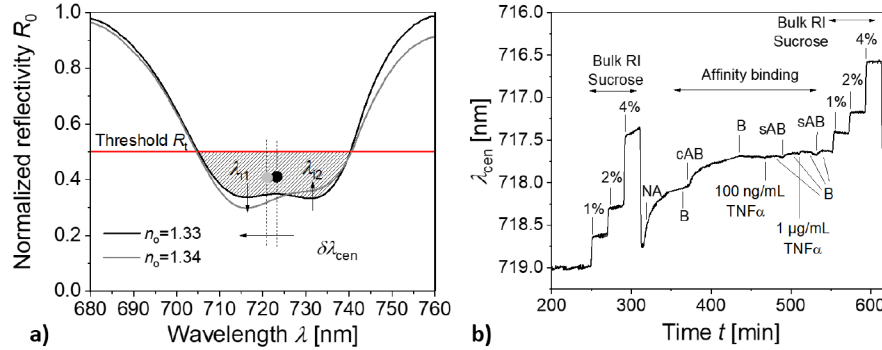


Fig. 5. a) Evaluation of the resonance variations due to refractive index changes by using the centroid method and b) example of the measured kinetics data for bulk refractive index changes δn_0 induced by a flow of buffer solution spiked with sucrose at 1%, 2% and 4% and for the affinity binding on the sensor surface. B indicates the rinsing with PBST.

Finally, the MPG sensor chip was used for the probing of affinity binding of biomolecules that constitute an assay for the detection of a protein biomarker TNF- α – human tumor necrosis factor alpha. Firstly, a solution with neutravidin – NA – dissolved in PBST at a concentration of 125 μ g/mL was flowed through the sensor for 45 min. The respective SPR sensor signal presented in Fig. 5(b) shows a gradual decrease of λ_{cen} by 0.75 nm due to the affinity binding of NA to biotin groups carried by the thiol SAM on the gold MPG surface. Then, biotinylated capture antibody – cAB – that is specific to TNF- α was immobilized from PBST solution spiked at a concentration of 2 μ g/mL that was flowed over the sensor surface for 45 min. Similar to the previous step, the affinity binding of cAB is manifested as a gradual decrease in λ_{cen} , which levels as a change of 0.30 nm. Afterwards, the sensor surface is used for the detection of TNF- α that was amplified by using a secondary antibody cAB that is also specific to TNF- α . The detection consisted of 15 min flow of TNF- α , 5 min rinsing with PBST, and additional 15 min binding of the sAB dissolved at 500 ng/mL in PBST. As seen in Fig. 5(b), a shift in λ_{cen} (0.028 nm) was measured for direct binding of the TNF- α at a concentration of 100 ng/mL, and an additional drop (0.04 nm) was observed after the sAB amplification. In the second step, the same assay was repeated for the TNF- α concentration increased to 1 μ g/mL and the affinity binding resulted in a stronger response (0.036 nm and 0.059 nm, respectively). Let us note that these values are not directly proportional to the TNF- α concentration in a liquid sample as the sensor surface binding capacity probably reached its saturation. At the end of the experiment, the calibration was repeated by changing the bulk refractive index n_0 with sucrose spiking of PBST, leading to similar shifts as at the start of the experiment.

4. Conclusions

The proposed concept of multi-period grating – MPG – was theoretically investigated and experimentally demonstrated to provide efficient means for the direct back-side excitation of propagating surface plasmons. Compared to alternative approaches based on long-range surface plasmons relying on low refractive index polymers and localized surface plasmons supported by arrays of metallic nanoparticles, the developed structures can be prepared without complex lithography steps and do not rely on expensive polymer materials. In conjunction with

advancements in the nanoimprint lithography that can be scaled up using roll-to-roll configuration, large areas carrying MPG structure can be prepared and exploited in various sensor modalities. The refractometric experiment and a model assay experiment confirm that the accuracy of the sensor configuration probed from the back-side sensor chip is similar to that measured for regular grating coupled SPR when the probing is performed through the analyzed liquid sample.

Funding

ESIF and MEYS (CZ.02.2.69/0.0/0.0/18_053/0016627); Lower Austria (WST3-F-5030820/010-2019); Österreichische Forschungsförderungsgesellschaft (861578).

Disclosures

The authors declare no conflicts of interest to this article.

References

1. J. Homola, "Surface plasmon resonance sensors for detection of chemical and biological species," *Chem. Rev.* **108**(2), 462–493 (2008).
2. M. F. Cardinal, E. V. Ende, R. A. Hackler, M. O. McAnally, P. C. Stair, G. C. Schatz, and R. P. Van Duyne, "Expanding applications of SERS through versatile nanomaterials engineering," *Chem. Soc. Rev.* **46**(13), 3886–3903 (2017).
3. M. Bauch, K. Toma, M. Toma, Q. Zhang, and J. Dostalek, "Plasmon-enhanced fluorescence biosensors: a review," *Plasmonics* **9**(4), 781–799 (2014).
4. D. Rodrigo, A. Tittl, N. Ait-Bouziad, A. John-Herpin, O. Limaj, C. Kelly, D. Yoo, N. J. Wittenberg, S. H. Oh, H. A. Lashuel, and H. Altug, "Resolving molecule-specific information in dynamic lipid membrane processes with multi-resonant infrared metasurfaces," *Nat. Commun.* **9**(1), 2160 (2018).
5. B. Liedberg, C. Nylander, and I. Lunström, "Surface plasmon resonance for gas detection and biosensing," *Sens. Actuators* **4**, 299–304 (1983).
6. J. Homola, J. Dostalek, S. F. Chen, A. Rasooly, S. Y. Jiang, and S. S. Yee, "Spectral surface plasmon resonance biosensor for detection of staphylococcal enterotoxin B in milk," *Int. J. Food Microbiol.* **75**(1-2), 61–69 (2002).
7. J. Dostalek, J. Homola, and M. Miler, "Rich information format surface plasmon resonance biosensor based on array of diffraction gratings," *Sens. Actuators, B* **107**(1), 154–161 (2005).
8. B. Spackova, P. Wrobel, M. Bockova, and J. Homola, "Optical Biosensors Based on Plasmonic Nanostructures: A Review," *Proc. IEEE* **104**(12), 2380–2408 (2016).
9. A. J. Haes and R. P. Van Duyne, "A nanoscale optical biosensor: Sensitivity and selectivity of an approach based on the localized surface plasmon resonance spectroscopy of triangular silver nanoparticles," *J. Am. Chem. Soc.* **124**(35), 10596–10604 (2002).
10. O. Kedem, A. Vaskevich, and I. Rubinstein, "Improved Sensitivity of Localized Surface Plasmon Resonance Transducers Using Reflection Measurements," *J. Phys. Chem. Lett.* **2**(10), 1223–1226 (2011).
11. J. A. Jackman, V. P. Zhdanov, and N. J. Cho, "Nanoplasmonic Biosensing for Soft Matter Adsorption: Kinetics of Lipid Vesicle Attachment and Shape Deformation," *Langmuir* **30**(31), 9494–9503 (2014).
12. J. Yamamichi, T. Ojima, M. Iida, K. Yurugi, T. Imamura, E. Ashihara, S. Kimura, and T. Maekawa, "Surface chemical approach to single-step measurement of antibody in human serum using localized surface plasmon resonance biosensor on microtiter plate system," *Anal. Bioanal. Chem.* **406**(18), 4527–4533 (2014).
13. M. Couture, K. K. Ray, H. P. Poirier-Richard, A. Crofton, and J. F. Masson, "96-Well Plasmonic Sensing with Nanohole Arrays," *ACS Sens.* **1**(3), 287–294 (2016).
14. D. M. Zhang, Y. L. Lu, Q. Zhang, Y. Yao, S. Li, H. L. Li, S. L. Zhuang, J. Jiang, G. L. Liu, and Q. J. Liu, "Nanoplasmonic monitoring of odorants binding to olfactory proteins from honeybee as biosensor for chemical detection," *Sens. Actuators, B* **221**, 341–349 (2015).
15. M. Vala, C. T. Ertsgaard, N. J. Wittenberg, and S. H. Oh, "Plasmonic Sensing on Symmetric Nanohole Arrays Supporting High-Q Hybrid Modes and Reflection Geometry," *ACS Sens.* **4**(12), 3265–3274 (2019).
16. D. Sarid, "Long range surface plasma waves on very thin metal films," *Phys. Rev. Lett.* **47**(26), 1927–1930 (1981).
17. N. C. Lindquist, T. W. Johnson, J. Jose, L. M. Otto, and S. H. Oh, "Ultrasoother metallic films with buried nanostructures for backside reflection-mode plasmonic biosensing," *Ann. Phys.* **524**(11), 687–696 (2012).
18. M. Vala and J. Homola, "Multiple beam interference lithography: A tool for rapid fabrication of plasmonic arrays of arbitrary shaped nanomotifs," *Opt. Express* **24**(14), 15656–15665 (2016).
19. G. Barbillon, "Plasmonic Nanostructures Prepared by Soft UV Nanoimprint Lithography and Their Application in Biological Sensing," *Micromachines* **3**(1), 21–27 (2012).
20. N. G. Quilis, M. Leveque, I. Khan, W. Knoll, S. Boujday, M. Lamy de la Chapelle, and J. Dostalek, "Tunable laser interference lithography preparation of plasmonic nanoparticle arrays tailored for SERS," *Nanoscale* **10**(21), 10268–10276 (2018).

21. H. Im, S. H. Lee, N. J. Wittenberg, T. W. Johnson, N. C. Lindquist, P. Nagpal, D. J. Norris, and S. H. Oh, "Template-Stripped Smooth Ag Nanohole Arrays with Silica Shells for Surface Plasmon Resonance Biosensing," *ACS Nano* **5**(8), 6244–6253 (2011).
22. N. Q. Quilis, M. van Dongen, P. Venugopalan, D. Kotlarek, C. Petri, A. M. Cencerrado, S. Stanesco, J. L. Toca Herrera, U. Jonas, M. Möller, A. Mourran, and J. Dostalek, "Actively tunable collective localized surface plasmons by responsive hydrogel membrane," *Adv. Opt. Mater.* **7**(15), 1900342 (2019).
23. I. Khan, H. Keshmiri, F. Kolb, T. Dimopoulos, and E. List-Kratochvil, "Plasmonic absorber based on multi-diffractive grating," *Adv. Opt. Mater.* **4**(3), 435–443 (2016).
24. S. Fossati, S. Hageneder, S. Menad, E. Mailart, and J. Dostalek, "Multiresonant plasmonic nanostructures for ultrasensitive fluorescence biosensing," *Nanophotonics* **9**(11), 3673–3685 (2020).
25. P. Adam, J. Dostalek, and J. Homola, "Multiple surface plasmon spectroscopy for study of biomolecular systems," *Sens. Actuators, B* **113**(2), 774–781 (2006).
26. G. G. Nenninger, M. Piliarik, and J. Homola, "Data analysis for optical sensors based on spectroscopy of surface plasmons," *Meas. Sci. Technol.* **13**(12), 2038–2046 (2002).
27. W. L. Barnes, T. W. Preist, S. C. Kitson, J. R. Sambles, N. K. Cotter, and D. J. Nash, "Photonic gaps in the dispersion of surface plasmons on gratings," *Phys. Rev. B* **51**(16), 11164–11167 (1995).
28. W. L. Barnes, T. W. Preist, S. C. Kitson, and J. R. Sambles, "Physical origin of photonic energy gaps in the propagation of surface plasmons on gratings," *Phys. Rev. B* **54**(9), 6227–6244 (1996).
29. D. Kotlarek, M. Vorobii, W. Ogieglo, W. Knoll, C. Rodriguez-Emmenegger, and J. Dostalek, "Compact Grating-Coupled Biosensor for the Analysis of Thrombin," *ACS Sens.* **4**(8), 2109–2116 (2019).